Cell

The Mad2 Conformational Dimer: Structure and Implications for the Spindle Assembly Checkpoint

Marina Mapelli,[1,*] Lucia Massimiliano,[1] Stefano Santaguida,[1] and Andrea Musacchio[1,2,*]
[1]Department of Experimental Oncology, European Institute of Oncology, Via Adamello 16, I-20139, Milan, Italy
[2]Research Unit of the Italian Institute of Technology at the Consortium for Genomic Technologies (Cogentech), Via Adamello 16, I-20139 Milan, Italy
*Correspondence: marina.mapelli@ifom-ieo-campus.it (M.M.), andrea.musacchio@ifom-ieo-campus.it (A.M.)
DOI 10.1016/j.cell.2007.08.049

SUMMARY

The 25 kDa Mad2 protein is a key player in the spindle assembly checkpoint, a safeguard against chromosome segregation errors in mitosis. Mad2 combines three unusual properties. First, Mad2 adopts two conformations with distinct topologies, open (O) and closed (C) Mad2. Second, C-Mad2 forms topological links with its two best-characterized protein ligands, Mad1 and Cdc20. Third, O-Mad2 and C-Mad2 engage in a "conformational" dimer that is essential for spindle checkpoint function in different organisms. The crystal structure of the O-Mad2–C-Mad2 conformational dimer, reported here, reveals an asymmetric interface that explains the selective dimerization of the O-Mad2 and C-Mad2 conformers. The structure also identifies several buried hydrophobic residues whose rearrangement correlates with the Mad2 topological change. The structure of the O-Mad2–C-Mad2 conformational dimer is consistent with a catalytic model in which a C-Mad2 template facilitates the binding of O-Mad2 to Cdc20, the target of Mad2 in the spindle checkpoint.

INTRODUCTION

The Mad2 protein is conserved in all eukaryotes (Musacchio and Salmon, 2007; Taylor et al., 2004). During mitosis, Mad2 and several other spindle assembly checkpoint (SAC) proteins are recruited to kinetochores, proteinaceous chromosomal scaffolds devoted to the capture of spindle microtubules (Cleveland et al., 2003; Musacchio and Salmon, 2007; Taylor et al., 2004). At kinetochores, the SAC proteins monitor the formation of stable kinetochore-microtubule attachments (the kinetochore fibers, or K-fibers), which are required for chromosome congression and alignment at the metaphase plate and in the subsequent separation of the sister chromatids at anaphase (Maiato et al., 2004).

The SAC targets Cdc20, an activator of the Anaphase Promoting Complex or Cyclosome (APC/C) (Peters, 2006). The Ubiquitin ligase activity of the APC/C is required to trigger anaphase and mitotic exit. By targeting Cdc20, the SAC keeps the APC/C in check and prevents its activation until all sister chromatid pairs are properly aligned at the metaphase plate (Peters, 2006). This condition satisfies the SAC, whose signal subsides, leading to APC/C activation and, after a cascade of molecular events, to the irreversible removal of sister chromatid cohesion (Peters, 2006).

Mad2 binds directly to Cdc20 and this interaction is essential for SAC function (Hwang et al., 1998; Kim et al., 1998; Luo et al., 2000; Sironi et al., 2001). The mechanism whereby Mad2 binds Cdc20 has been intensely investigated (Nasmyth, 2005). The ~200-residue sequence of Mad2 folds as a HORMA domain (Aravind and Koonin, 1998). The HORMA domain of Mad2 adopts two distinct conformations. A conformation known as C-Mad2 is observed when Mad2 is bound to Cdc20 (Luo et al., 2002; Sironi et al., 2002). This binding mode, which will be described in more detail later on, entails a topological connection in which the Mad2-binding site of Cdc20 is held in a binding pocket of Mad2 by a mobile element known as the "safety belt" (Luo et al., 2002; Sironi et al., 2002). Kinetochores devoid of microtubules retain a tight complex of Mad2 with another SAC protein named Mad1 (Chen et al., 1999, 1998; Chung and Chen, 2002; De Antoni et al., 2005a; Luo et al., 2002; Martin-Lluesma et al., 2002; Nasmyth, 2005; Sironi et al., 2002; Vink et al., 2006). The way in which Mad1 binds Mad2 is equivalent to that of Cdc20, in that Mad1 binds to the same ligand-binding site of C-Mad2. There is now substantial evidence that the tight Mad1–Mad2 complex, which is further stabilized by 2:2 tetramerization, does not significantly dissociate during checkpoint activation (De Antoni et al., 2005a; Shah et al., 2004; Vink et al., 2006). Its function at the kinetochore is to recruit from the mitotic cytosol a different conformer of Mad2, known as O-Mad2 (or N1 Mad2), for

Cdc20 binding (De Antoni et al., 2005a; Vink et al., 2006). The structure of O-Mad2 has also been characterized. Relative to its position in C-Mad2, the "safety belt" of O-Mad2 occupies a resting position at the opposite end of an exposed β sheet of Mad2 (Luo et al., 2000, 2004). Kinetochore recruitment of cytosolic O-Mad2 entails its dimerization with the C-Mad2 moiety of the Mad1–Mad2 complex (De Antoni et al., 2005a, 2005b). The exact significance of the O-Mad2–C-Mad2 dimerization is unclear (Nasmyth, 2005), but it seems plausible that after docking onto C-Mad2, the O-Mad2 conformer bound to C-Mad2 undergoes a conformational change into an "active" form that can bind more readily to Cdc20. Like Mad2, also Cdc20 is enriched at kinetochores, where it binds to an unknown receptor (Kallio et al., 1998). The logic of this network is that the conformational dimerization of O-Mad2 with Mad1-bound C-Mad2 facilitates the complex conformational rearrangement required to bind Cdc20, possibly through the creation of a structural intermediate (Figure S1 in the Supplemental Data available with this article online). This model is named "Mad2 template" model, as it suggests that C-Mad2 bound to Mad1 acts as a template to generate C-Mad2 bound to Cdc20 (De Antoni et al., 2005a; Nasmyth, 2005; Yu, 2006).

Additional negative and positive regulators, including $p31^{comet}$, UbcH10, and USP44, have been recently identified and shown to be important for regulating the stability of the Mad2–Cdc20 complex (Habu et al., 2002; Mapelli et al., 2006; Reddy et al., 2007; Stegmeier et al., 2007; Xia et al., 2004). Like O-Mad2, $p31^{comet}$ binds specifically and with high-affinity to C-Mad2, and competes with the association of O-Mad2 to C-Mad2 (Mapelli et al., 2006; Vink et al., 2006; Xia et al., 2004). Thus, the ability of $p31^{comet}$ to negatively regulate the SAC might be based on its ability to interfere with the interaction of O-Mad2 with C-Mad2. So far, the structural bases of this property of $p31^{comet}$ have not been clarified.

The structure of the core element of the "Mad2 template" model, the O-Mad2–C-Mad2 dimer, has not been described previously. Here, we report the crystal structure of the O-Mad2–C-Mad2 complex and discuss its properties and implications for the SAC. In an accompanying paper in this issue of *Cell*, Luo, Yu, and coworkers report the structure of $p31^{comet}$ bound to C-Mad2 (Yang et al., 2007). They find that $p31^{comet}$ is structurally related to Mad2, and that its complex with C-Mad2 bears striking similarities with the structure of the O-Mad2-C-Mad2 dimer. Together, these structures provide a framework to understand the implications of Mad2 dimerization in the SAC and describe what is probably an unprecedented mechanism for protein dimerization. To harmonize the description of Mad2 conformers in this paper and in Yang et al. (2007), the name open-Mad2 (abbreviated as O-Mad2) will be used to describe structures previously described as O-Mad2 or N1-Mad2. The name closed-Mad2 (abbreviated as C-Mad2) will be used to describe structures previously referred to as C-Mad2, N2-Mad2 and N2′-Mad2 (Luo et al., 2000, 2002, 2004; Musacchio and Salmon, 2007; Sironi et al., 2002; Yu, 2006). N2-Mad2 has been used to describe an "empty" C-Mad2 conformer devoid of Mad2 ligands (Luo et al., 2004; Yu, 2006). We will refer to the "empty" form of C-Mad2 as "unliganded C-Mad2." We also propose to name the hypothetical active form of Mad2, previously often indicated as $Mad2^{*}$, as intermediate-Mad2 (I-Mad2).

RESULTS AND DISCUSSION

Architecture of the O-Mad2–C-Mad2 Conformational Dimer

Our previous attempts to crystallize the O-Mad2–C-Mad2 complex were unsuccessful, possibly because the interaction is highly dynamic (Mapelli et al., 2006; Vink et al., 2006). To overcome this problem, we tried to create a "stabilized" form of O-Mad2. For this, we deleted residues 109–117 from the loop that connects strand β5 to helix αC (the β5-αC loop) of human Mad2 and substituted them with a Gly-Ser-Gly triplet (the resulting mutant is named $Mad2^{LL}$, for loop-less. The reason why this mutant is stabilized as O-Mad2 is explained below). To generate C-Mad2, we "closed" full-length wild-type Mad2 ($Mad2^{wt}$) with Mad2-binding peptide 1 (MBP1), a 12-residue peptide (sequence Ser-Trp-Tyr-Ser-Tyr-Pro-Pro-Pro-Gln-Arg-Ala-Val) mimicking the consensus Mad2-binding motifs of Mad1 and Cdc20 (Luo et al., 2002). In isolation, $Mad2^{LL}$ and the $Mad2^{wt}$–MBP1 complex eluted from a size-exclusion chromatography (SEC) column between the 44-kDa and 17-kDa markers, i.e., as monomers (Figure 1A; note that the 12-residue MBP1 peptide does not contribute significantly to the elution of C-Mad2–MBP1). A stoichiometric combination of $Mad2^{LL}$ and $Mad2^{wt}$–MBP1 generated a $Mad2^{LL}$–$Mad2^{wt}$–MBP1 complex eluting near the 44 kDa marker (Figure 1A). In the $Mad2^{wt}$–MBP1 complex, MBP1 is embedded as an additional element of the secondary structure of C-Mad2 (see below). Therefore, we will often refer to the $Mad2^{wt}$–MBP1 dimer simply as C-Mad2, and to its complex with O-Mad2 as a dimer (rather then a trimer).

We crystallized $Mad2^{LL}$–$Mad2^{wt}$–MBP1 and collected X-ray diffraction data to 2.9 Å resolution. The structure was determined by Molecular Replacement as described in Experimental Procedures. The model, which has been refined to a free R-factor of 27.4%, displays good geometrical parameters (Table 1). The structure confirms that $Mad2^{LL}$ and $Mad2^{wt}$–MBP1 form an O-Mad2–C-Mad2 conformational dimer (Figures 1B–1D). The topological differences between the O-Mad2 and C-Mad2 conformers in the dimer reside in the N- and C-terminal regions. In O-Mad2 ($Mad2^{LL}$), the first part of the N-terminal 15-residue segment is disordered, and the second part forms the short β1-strand (Figure 1B). This is positioned in a shallow cleft between the β5-strand and the αC helix (Figures 1C–1E). Relative to the β1-strand, the β7-β8 hairpin at the C terminus of Mad2 (red) occupies the opposite end of the exposed β sheet of O-Mad2, away from the interface with C-Mad2. In the C-Mad2 protomer, the N-terminal

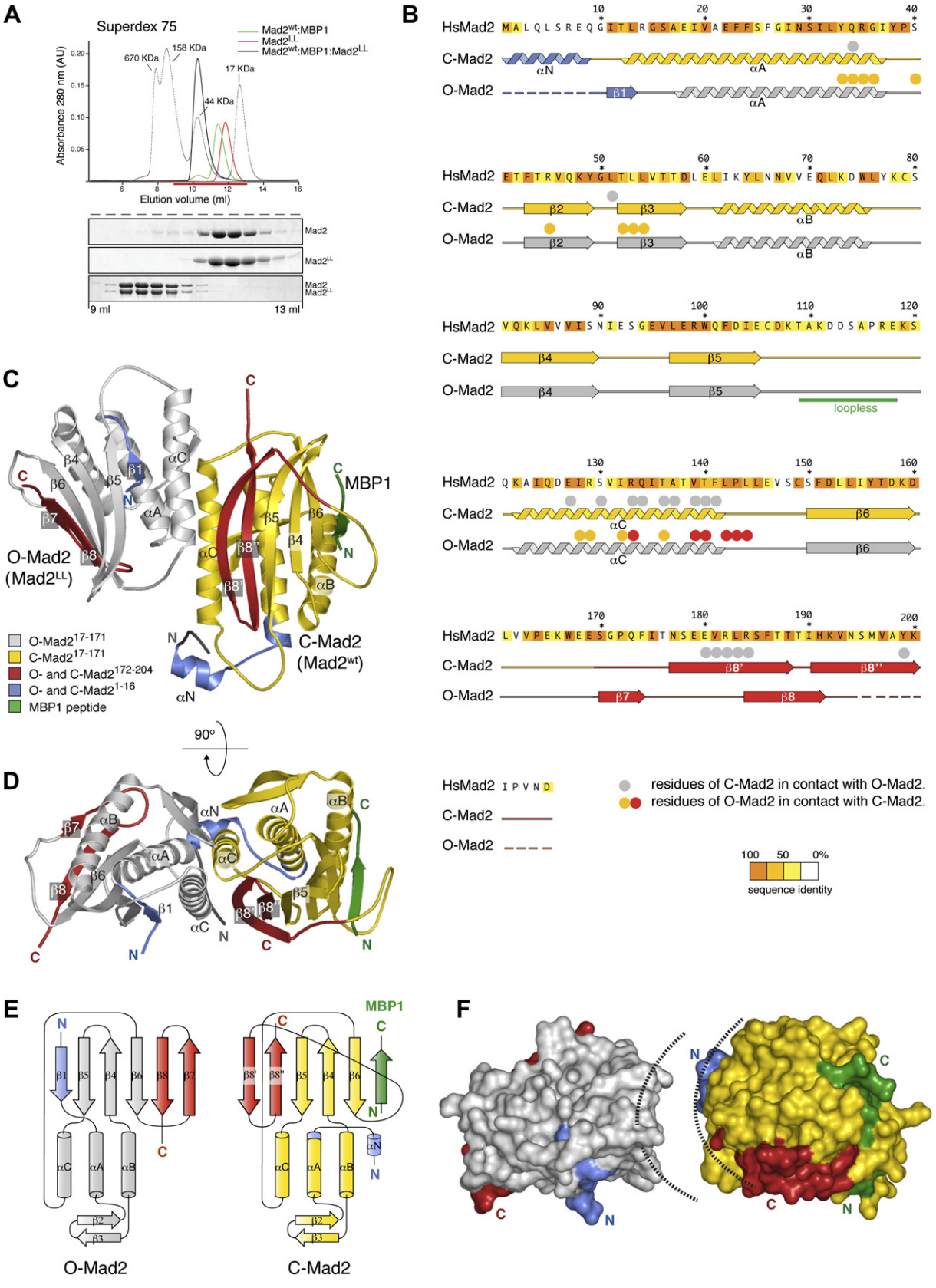
A
Superdex 75
Mad2wt:MBP1
Mad2LL
Mad2wt:MBP1:Mad2LL
670 KDa
158 KDa
44 KDa
17 KDa
Absorbance 280 nm (AU)
Elution volume (ml)
Mad2
Mad2LL
9 ml
13 ml
B
HsMad2
C-Mad2
O-Mad2
C
O-Mad2 (Mad2LL)
C-Mad2 (Mad2wt)
MBP1
O-Mad2 17-171
C-Mad2 17-171
O- and C-Mad2 172-204
O- and C-Mad2 1-16
MBP1 peptide
90°
D
E
O-Mad2
C-Mad2
MBP1
F
loopless
residues of C-Mad2 in contact with O-Mad2.
residues of O-Mad2 in contact with C-Mad2.
100 50 0%
sequence identity

Table 1. Data Collection and Refinement Statistics

Data Collection	MBP1–Mad2^{wt}–Mad2^{LL}
Space group	$P2_12_12_1$
Beamline/Synchroton	ID14-2/ESRF
Wavelength (Å)	0.933
Unit cell dimensions (Å)	
	112.58
	111.31
	131.76
Resolution (Å)[a]	30.0 – 2.9 (3.0 – 2.9)
Total observations	597,084
Unique reflections	37,591
Data completeness (%)	100.0 (100.0)
Rsym (%)[b]	11.6 (45.1)
I/σI	16.2 (4.4)
Refinement	
Resolution range (Å)	30.0 – 2.9
Rconv[c]/Rfree[d]	23.4/27.4
Number of protein atoms	9642
Number of solvent atoms	6
Rmsd bond lengths (Å)	0.018
Rmsd bond angles (°)	2.0
Mean B-factor protein (Å^2)	39.3

[a] Values in parentheses refer to the outer resolution shell.
[b] $R_{symm} = \sum| I - < I > |/\sum I$, where I is the observed intensity of a reflection and < I > is the average intensity obtained from multiple observations of symmetry-related reflections.
[c] $R_{conv} = \sum ||F_o| - |F_c||/\sum |F_o|$, where F_o and F_c are the observed and calculated structure factor amplitudes respectively.
[d] R_{free} is equivalent to R_{conv} for a 5% subset of reflections not used in the refinement.

segment extends the αA helix and forms an additional short helix (αN, Figure 1B). The C-terminal tail of C-Mad2 (the safety belt, containing the two strands β8′-β8″), rather than the β1-strand, occupies the cleft between the β5-strand and the αC helix. In this new position, obtained by traversing the entire exposed β sheet of C-Mad2, the safety belt is at the interface with O-Mad2, to which it contributes several contacts. At the opposite edge of the exposed β sheet of C-Mad2, the MBP1 peptide augments the β sheet after pairing with the β6-strand, and becomes partially buried under the Mad2 safety belt, as described previously (Luo et al., 2002; Sironi et al., 2002). The topological link of MBP1 with C-Mad2 is already evident in Figure 1F, which shows that the MBP1 chain (green) is embraced by the safety belt. The Mad2-binding segments of Mad1 and Cdc20, which bind to the same pocket of Mad2 (Luo et al., 2002; Sironi et al., 2002), are flanked on either side by hundreds of residues (Figure S1). This explains why the association with, and dissociation from, Mad2 of these ligands implies the opening of the safety belt (Sironi et al., 2002).

The dimerization of O-Mad2 and C-Mad2–MBP1 reported here is structurally compatible with the binding of O-Mad2 to the Mad1–C-Mad2 complex (Sironi et al., 2002). If we superimpose the C-Mad2 moiety of the O-Mad2–C-Mad2 dimer on the C-Mad2 moiety of the Mad1–C-Mad2 complex (PDB ID code 1GO4), O-Mad2 nicely fits on the Mad1–C-Mad2 complex without steric clashes with Mad1 (Figure S1), in agreement with previous biochemical analyses demonstrating a physical interaction between O-Mad2 and the Mad1–C-Mad2 complex (De Antoni et al., 2005a).

The Dimer Interface

The structure of the O-Mad2–C-Mad2 conformational dimer reveals that the interaction surface is asymmetric, rather than pseudo-symmetric as previously proposed based on modeling (Mapelli et al., 2006). The interaction buries a total of 1960 Å^2. Several residues at the O-Mad2–C-Mad2 interface, including Arg133, Gln134, Thr140, Phe141 and Arg184, are evolutionarily invariant or well conserved (Figure 1B). Single alanine mutants of these residues in *Saccharomyces cerevisiae* are unable to sustain the SAC in a *MAD2*-deficient strain, supporting the proposition that the function of Mad2 dimerization in the SAC is conserved in evolution (Mapelli et al., 2006; Nezi et al., 2006). With an asymmetric interaction surface, equivalent residues of O-Mad2 and C-Mad2 face different chemical environments. For instance, Arg133$^{C\text{-}Mad2}$ forms a hydrogen bond with the backbone oxygen of Gln34$^{O\text{-}Mad2}$, while the side chain of Arg133$^{O\text{-}Mad2}$ stacks against the aromatic ring of Phe141$^{C\text{-}Mad2}$.

Figure 1. Structure of the O-Mad2–C-Mad2 Dimer

(A) Mad2^{LL} (red trace) and Mad2^{wt}–MBP1 12-residue peptide complex (green trace) elute between the 44 kDa and 17 kDa markers from a Superdex-75 SEC column. When combined stoichiometrically, these proteins form a ternary complex that elutes with the 44-kDa marker. The content of fourteen 300-μl fractions between 9 and 13.2 ml was analyzed by SDS-PAGE and Coomassie staining.

(B) Sequence and secondary structure of O-Mad2 and C-Mad2. Mad2 residues are colored according to the conservation bar shown at the bottom of the panel, which was calculated based on an alignment of 15 sequences (Mapelli et al., 2006). The circles mark C-Mad2 and O-Mad2 residues at the dimer interface, respectively, and their color code refers to the location of the contact on the cognate Mad2.

(C and D) Ribbon models of the Mad2 conformational dimer viewed at the indicated rotations.

(E) Topology diagram of O-Mad2 and C-Mad2. In C-Mad2, the two strands β8′–β8″ are extensions in opposite directions of the β8 strand of O-Mad2, which justifies the nomenclature β8′–β8″ for these strands.

(F) Surface models of O-Mad2 and C-Mad2, oriented as in panel (D), have been parted to show the concavity and convexity of the binding surfaces. Figures were made with Pymol (http://www.pymol.org) and Adobe Illustrator.

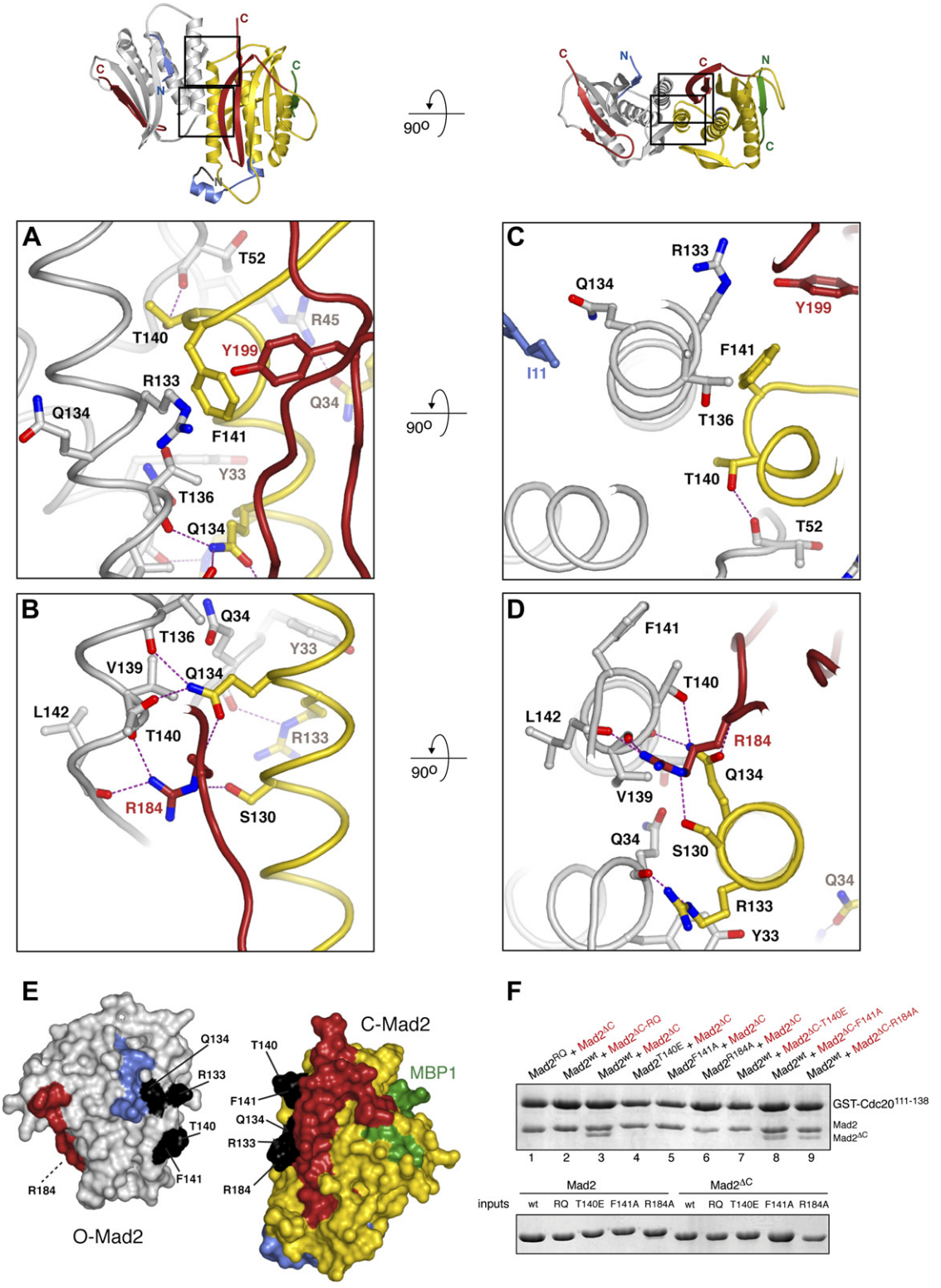

Figure 2. Analysis of the Asymmetric Dimer Interface

(A–D) Enlarged views of the dimer interface roughly corresponding to the boxes on the dimer shown in the upper left and upper right part of the figure. Panels (A), (C), (B), and (D) are related by 90° rotations. Color-coding for all carbon atoms is as in Figure 1; nitrogen, blue; oxygen, red. Hydrogen bonds are dashed purple lines.

Phe141$^{O\text{-}Mad2}$, on the other hand, is not engaged in interactions with C-Mad2 (Figures 2A–2D). Gln134$^{C\text{-}Mad2}$ is hydrogen-bonded to the side chain of Thr140$^{O\text{-}Mad2}$ and to the carbonyl group of Thr136$^{O\text{-}Mad2}$. Conversely, Gln134$^{O\text{-}Mad2}$ points away from the interaction surface, while Thr140$^{C\text{-}Mad2}$ forms a polar interaction with Thr52$^{O\text{-}Mad2}$ that anchors the β hairpin of O-Mad2 to the αC helix of C-Mad2. The β8′-β8″ hairpin of C-Mad2 interacts with O-Mad2 via Arg184$^{C\text{-}Mad2}$, which is hydrogen-bonded to the carbonyls of Val139$^{O\text{-}Mad2}$ and Leu142$^{O\text{-}Mad2}$, and via a stacking interaction of Tyr199$^{C\text{-}Mad2}$ with Arg133$^{O\text{-}Mad2}$ (Figures 2A–2D). In O-Mad2, Arg184 is far from the surface that contacts C-Mad2 (Figure 2E).

With an asymmetric interaction surface, certain residues are only required for binding on one of the two conformers. For instance, the structure predicts that the side chains of Phe141 and Arg184 are required for the interaction of C-Mad2 with O-Mad2, but should be dispensable for the interaction of O-Mad2 with C-Mad2. To test this, we carried out a binding assay that detects the binding of Mad2 to the Mad2-binding motif of human Cdc20 (Cdc20$^{111–138}$) and that also discriminates the effects of mutations on the ability of O- and C-Mad2 to form dimers (De Antoni et al., 2005a; Mapelli et al., 2006) (Figure 2F). Consistently with the structure of the O-Mad2–C-Mad2 complex, C-Mad2 versions of the single alanine point mutants of residues Phe141 or Arg184 (Figure 2F, lanes 5 and 6) prevented the binding of Mad2$^{\Delta C}$, a deletion mutant lacking 10 residues from the Mad2 C terminus, and that, like Mad2^{LL}, is a "locked" O-Mad2 conformer (Luo et al., 2000; Sironi et al., 2002). The same mutations in O-Mad2 did not significantly alter the binding to C-Mad2^{wt} (lanes 8 and 9). The effects of mutating Arg184 demonstrate that the C-terminal region of C-Mad2 is essential for conformational dimerization. In agreement with our analysis, we have previously shown that alanine mutants of Arg133 weaken binding both on the O-Mad2 and on the C-Mad2 surface (De Antoni et al., 2005b). Like Arg133, also Thr140 is engaged - in different chemical environments – in the binding interface of both conformers. Point mutants of this residue effectively impaired dimerization both in the context of O-Mad2 and of C-Mad2 (lanes 1, 2, 4, and 7). Altogether, these results are fully consistent with the revelation from the crystal structure that the O-Mad2–C-Mad2 interface is intrinsically asymmetric. As the structure-based mutational analysis in Figure 2F was carried out with O-Mad2$^{\Delta C}$, whose β5-αC loop is intact, we believe that the observed position of the αC helix is not significantly affected by the deletion of the β5-αC loop in Mad2^{LL}.

Topology of the Mad2 Conversion

The structures of O-Mad2 and C-Mad2 suggest that displacement of the β1-strand is a prerequisite for relocating the β7-β8-harpin of O-Mad2 across the β sheet to create C-Mad2 (Figure 3A). In C-Mad2, the 1–15 segment (containing β1) appears as an extension of the αA helix. This rearrangement requires that the 1–15 segment be withdrawn beneath the β5-αC loop (Figure 3A). A tighter loop could lock O-Mad2 and prevent the transition. Indeed, the Mad2^{LL} mutant, which has a shortened β5-αC loop, stably adopts the O-Mad2 conformation. Like Mad2$^{\Delta C}$, Mad2^{LL} is unable to bind Cdc20 (Figure 3B, lanes 2 and 3) or Mad1 (data not shown and ref. Sironi et al., 2001). Thus, the length of the β5-αC loop of Mad2 is important for relocating the N-terminal segment of Mad2, which is in turn required for relocating the C-terminal "safety belt" (Figure 3A). As stable O-Mad2 conformers, Mad2$^{\Delta C}$ and Mad2^{LL} bind C-Mad2 normally (Figure 3B, lanes 6 and 7), in agreement with the observation that neither the C-terminal region of O-Mad2 nor the β5-αC loop of O-Mad2, are engaged in dimerization (Figure 1). Thus, Mad2^{LL} and Mad2$^{\Delta C}$ are both stabilized as O-Mad2 but are both endowed with a fully functional O-Mad2 interface for C-Mad2 binding, which is at the basis of the dominant-negative effects of Mad2$^{\Delta C}$ (Canman et al., 2002). So far, we have only been able to crystallize a conformational dimer containing Mad2^{LL}, possibly because the deletion of the β5-αC loop restricts the mobility of the N-terminal region in Mad2^{LL}.

In agreement with the idea that Mad2 closure might be facilitated in the absence of β1, Mad2$^{\Delta N15}$, a Mad2 mutant lacking the first 15 residues of Mad2, has been proposed to exist predominantly as a C-Mad2 conformer, even in the absence of ligands such as Mad1 or Cdc20 (Mapelli et al., 2006). This form of unliganded C-Mad2, first described by Yu and colleagues (Luo et al., 2004), is characterized by a closed position of the safety belt despite the fact that the Mad2 ligand-binding site is devoid of Mad2 ligands (Luo et al., 2004). To confirm that Mad2$^{\Delta N15}$ folds as unliganded C-Mad2, we took advantage of the previous observation that the O-Mad2 and C-Mad2 conformers can be discriminated based on their profile of elution from an anion exchange (AE) column (Luo et al., 2004). In agreement with these previous studies, all known O-Mad2 mutants show the same profile of elution from a Resource-Q

(E) Surface view of a broken dimer colored as in Figure 1 with "asymmetric" residues shown in black.

(F) GST-Cdc20$^{111–138}$ on GSH beads was incubated with the Mad2 species labeled in black on the upper part of the panel. After a 1 hr incubation, the excess Mad2 was washed out and the Mad2 species labeled in red were added for a second 1 hr incubation. After a washing step, SDS-PAGE and Coomassie staining were used to visualize bound species. Mad2$^{R133E\text{-}Q134A}$ (lane 1) is a control Mad2 that binds Cdc20 but is impaired in its interaction with O-Mad2 (De Antoni et al., 2005a). The same mutations in the frame of O-Mad2 prevent binding to wild-type C-Mad2 (lane 2). Mad2$^{\Delta C}$ acts as a "wild type" form of O-Mad2, and binds to the GST-Cdc20$^{111–138}$–Mad2 complex (lane 3). C-Mad2 mutants T140E, F141A and R184A do not bind Mad2$^{\Delta C}$ (lanes 4–6). O-Mad2 mutant T140E failed to bind C-Mad2^{wt} (lane 7). The O-Mad2 F141A and R184A mutations did not prevent O-Mad2 from binding C-Mad2^{wt} (lanes 8 and 9) demonstrating that they act asymmetrically on the opposing surfaces. The protein samples used in these experiments are also shown.

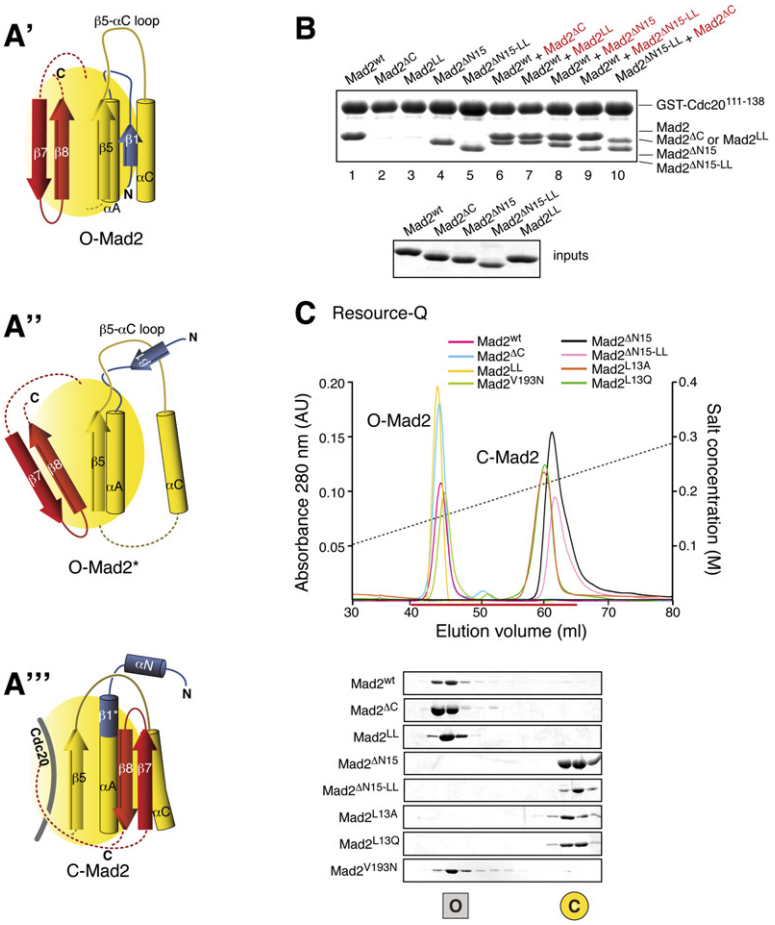

Figure 3. Topology of the Mad2 Conversion

(A′–A‴) Schematic view of the Mad2 closure showing selected elements of the secondary structure. In (A′), the N-terminal (blue) and C-terminal (red) regions of O-Mad2 are still in place. The conversion in (A″) requires that the N-terminal β1-strand is removed to allow the relocation of the C-terminal region. Eventually, the N-terminal region needs to relocate at the N-terminus of Mad2, and the passage requires an "opening" through the β5-αC loop. C-Mad2 is schematized in (A‴).

(B) The Cdc20-binding and dimerization properties of different "topological" mutants of Mad2 were tested in the same binding assay already introduced in Figure 2, panel F. Mad2^{wt} binds GST-Cdc20$^{111–138}$ (lane 1) but the constitutively locked O-Mad2 forms Mad2$^{\Delta C}$ and Mad2^{LL} do not (lanes 2 and 3). Mad2$^{\Delta N15}$ and Mad2$^{\Delta N15\text{-}LL}$ bind GST-Cdc20$^{111–138}$, indicating that they can adopt a closed Mad2 conformation (lanes 4 and 5). Like Mad2$^{\Delta C}$ and Mad2^{LL} (lanes 6 and 7), Mad2$^{\Delta N15}$ and Mad2$^{\Delta N15\text{-}LL}$ can also adopt the O-Mad2 conformation to bind bind C-Mad2^{wt} (lanes 6 and 7).

(C) Anion exchange chromatography separates monomeric O-Mad2 from C-Mad2 (see also Figure S2). Different Mad2 mutants with similar isoelectric points (Table S1) elute in a "conformation-sensitive" way from an anion-exchange column. Mad2^{wt}, Mad2$^{\Delta C}$, Mad2^{LL}, and Mad2^{V193N} eluted as O-Mad2 species. Mad2$^{\Delta N15}$, Mad2$^{\Delta N15\text{-}LL}$, Mad2^{L13A} and Mad2^{L13Q} elute as C-Mad2. Eluted fractions were collected and analyzed by SDS-PAGE.

AE column (Figure 3C and data not shown). Conversely, Mad2$^{\Delta N15}$ elutes at higher salt concentrations, in agreement with the idea that this mutant folds preferentially as unliganded C-Mad2. Indeed, we have shown previously that Mad2$^{\Delta N15}$ dimerizes with O-Mad2, as expected for a protomer in the closed conformation (Mapelli et al., 2006). The conditions for the validity of the AE assay are described in more detail in the Experimental Procedures section, in the legend of Figure S2, and in Table S1.

In summary, our data show that in the absence of the first fifteen N-terminal residues, Mad2 (Mad2$^{\Delta N15}$) prefers an unliganded C-Mad2 conformation, but this preference does not imply that unliganded C-Mad2 is the more stable conformer of the intact protein. Indeed, Mad2^{wt} eluted as an O-Mad2 conformer under the conditions of our assay (Figure 3C). Loss of the N-terminal region is likely to affect the stability of the Mad2 hydrophobic core, as explained below. Mad2$^{\Delta N15}$ also retained the ability to bind GST-Cdc20$^{111–138}$ (Figure 3B, lane 4). Although the re-opening of the C-terminal tail is slow (Luo et al., 2004), this observation is consistent with the time scale of our binding experiments (1 hr at 20°C).

If the deletion of the β5-αC loop restricts the mobility of the N-terminal region in Mad2^{LL}, generating a barrier to Mad2 closure, one would predict that the deletion of the Mad2 N-terminal region from Mad2^{LL} should suppress the inability to reposition the β7-β8 hairpin to form C-Mad2. To test this, we created the double deletion mutant Mad2$^{\Delta N15\text{-}LL}$. Consistent with our prediction, Mad2$^{\Delta N15\text{-}LL}$ prefers the C-Mad2 conformation (Figure 3C). Like Mad2$^{\Delta N15}$, Mad2$^{\Delta N15\text{-}LL}$ also binds to Cdc20$^{111–138}$ (Figure 3B, lane 5). Once bound to GST-Cdc20$^{111–138}$, Mad2$^{\Delta N15}$ (data not shown) and Mad2$^{\Delta N15\text{-}LL}$ behave essentially as wild-type C-Mad2 species in terms of O-Mad2 binding (Figure 3B, lane 10), in agreement with the fact that the N-terminal segment of C-Mad2 is not involved at the dimer interface (Figure 1B). Although these results do not clarify the exact order of modifications required to create C-Mad2 from O-Mad2, they indicate that the removal of the N-terminal region of Mad2 from the position it occupies in O-Mad2 and its relocation through the β5-αC loop are prerequisite to forming C-Mad2.

Conversion of the Mad2 Core

The substitution of the β1 strand of O-Mad2 with the β8′-β8″ hairpin of C-Mad2 involves a modification of the Mad2 hydrophobic core (Figures 4A–4C). In O-Mad2,

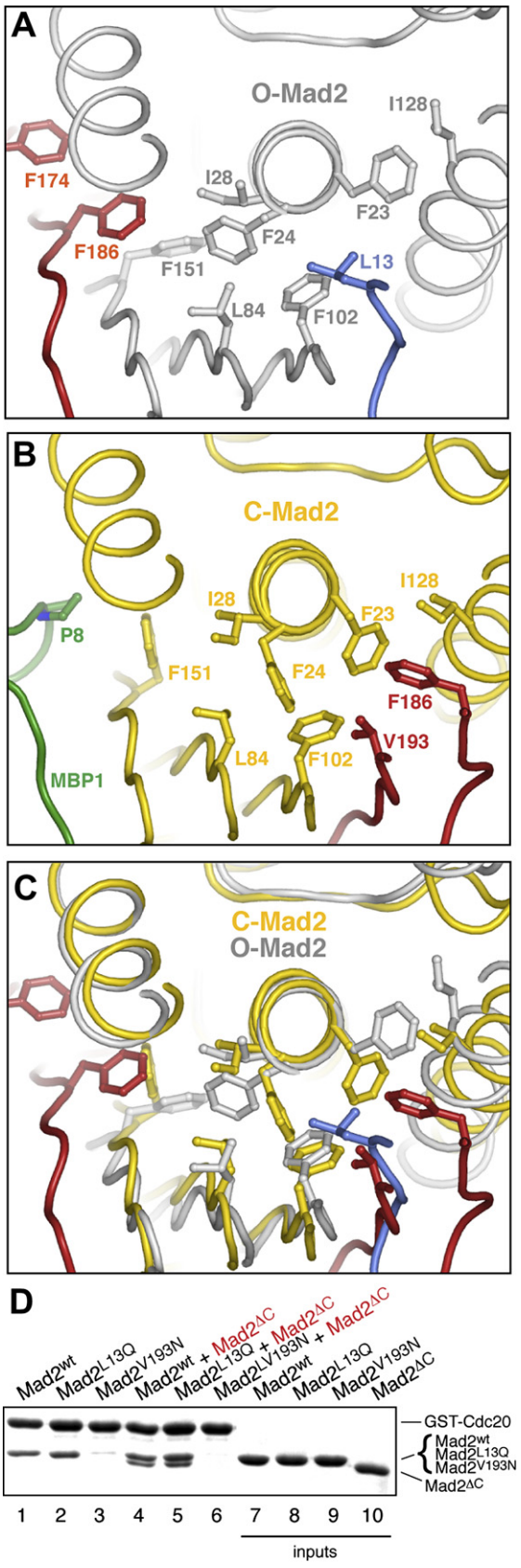

the side chain of Leu13 (in β1) inserts between the side chains of Phe23 and Phe24 of the αA helix (Figure 4A). Displacement of Leu13 from this site in C-Mad2 correlates with rotation of the side chains of Phe23 and Phe24 (Figure 4B). In C-Mad2, these side chains are in van der Waals contact with the side chains of Phe186 and Val193 in the β8′-β8″ hairpin (Figure 4B). To test the contribution of Leu13 to the stability of O-Mad2, we mutated it to Ala (Mad2^{L13A}) or to Gln (Mad2^{L13Q}) and analyzed the conformation of the resulting mutants. Strikingly, Mad2^{L13A} and Mad2^{L13Q} preferred the C-Mad2 conformation, recapitulating the effects of the "topological" mutants Mad2$^{\Delta N15}$ and Mad2$^{\Delta N15\text{-}LL}$ (Figure 3C). Like Mad2$^{\Delta N15}$ and Mad2$^{\Delta N15\text{-}LL}$, Mad2^{L13A} and Mad2^{L13Q} retained the ability to bind GST-Cdc20$^{111–138}$ (Figure 4D and data not shown). On the opposite front, Val193 is expected to play a prominent role in stabilizing C-Mad2, because its aliphatic side chain is exposed to solvent in O-Mad2 but is buried in the hydrophobic core of C-Mad2 (Figure 4B). Accordingly, mutation of Val193 into the polar residue Asn (Mad2^{V193N}) generates a mutant that is locked as O-Mad2 (Figure 3C), and is totally defective in Cdc20 binding (Figure 4D).

The O-Mad2–C-Mad2 and p31^{comet}–C-Mad2 Dimers Compared

The structure of the p31^{comet}–C-Mad2 dimer (Yang et al., 2007) reveals striking similarities with the structure of the O-Mad2–C-Mad2 dimer (Figures 5A and 5B). As described more thoroughly in the accompanying paper by Yang et al. (2007), p31^{comet} structurally resembles Mad2, and it binds to an area of the C-Mad2 surface that largely overlaps with that bound by O-Mad2. As p31^{comet} acts as a negative regulator of the SAC, the structure immediately suggests that p31^{comet} is likely to act by direct competition with the interaction of O-Mad2 with C-Mad2, as previously proposed (De Antoni et al., 2005a; Habu et al., 2002; Mapelli et al., 2006; Vink et al., 2006; Xia et al., 2004).

Besides the overall similarity, significant differences in the two dimeric structures provide possible clues to understand the structural conversion of Mad2. After superposition of the (essentially identical) C-Mad2 moieties of the two complexes, it appears that p31^{comet} covers a slightly larger area of the C-Mad2 surface relative to

Figure 4. Hydrophobic Core of Mad2 in the Conversion

(A) Hydrophobic core of O-Mad2.

(B) Hydrophobic core of C-Mad2.

(C) Superposition of hydrophobic cores of O-Mad2 and C-Mad2 showing differences in the choice of rotamers.

(D) The Cdc20-binding and dimerization properties of different "topological" mutants of Mad2 were tested in the same binding assay already introduced in Figure 2F. Mad2^{L13Q} and Mad2^{V193N} (lanes 2 and 3) mimic Mad2$^{\Delta N15}$ and Mad2$^{\Delta C}$, respectively, in their ability (or lack thereof) to bind GST-Cdc20$^{111–138}$, indicating that L13 and V193 play prominent functions for the stabilization of the O-Mad2 and C-Mad2 topologies.

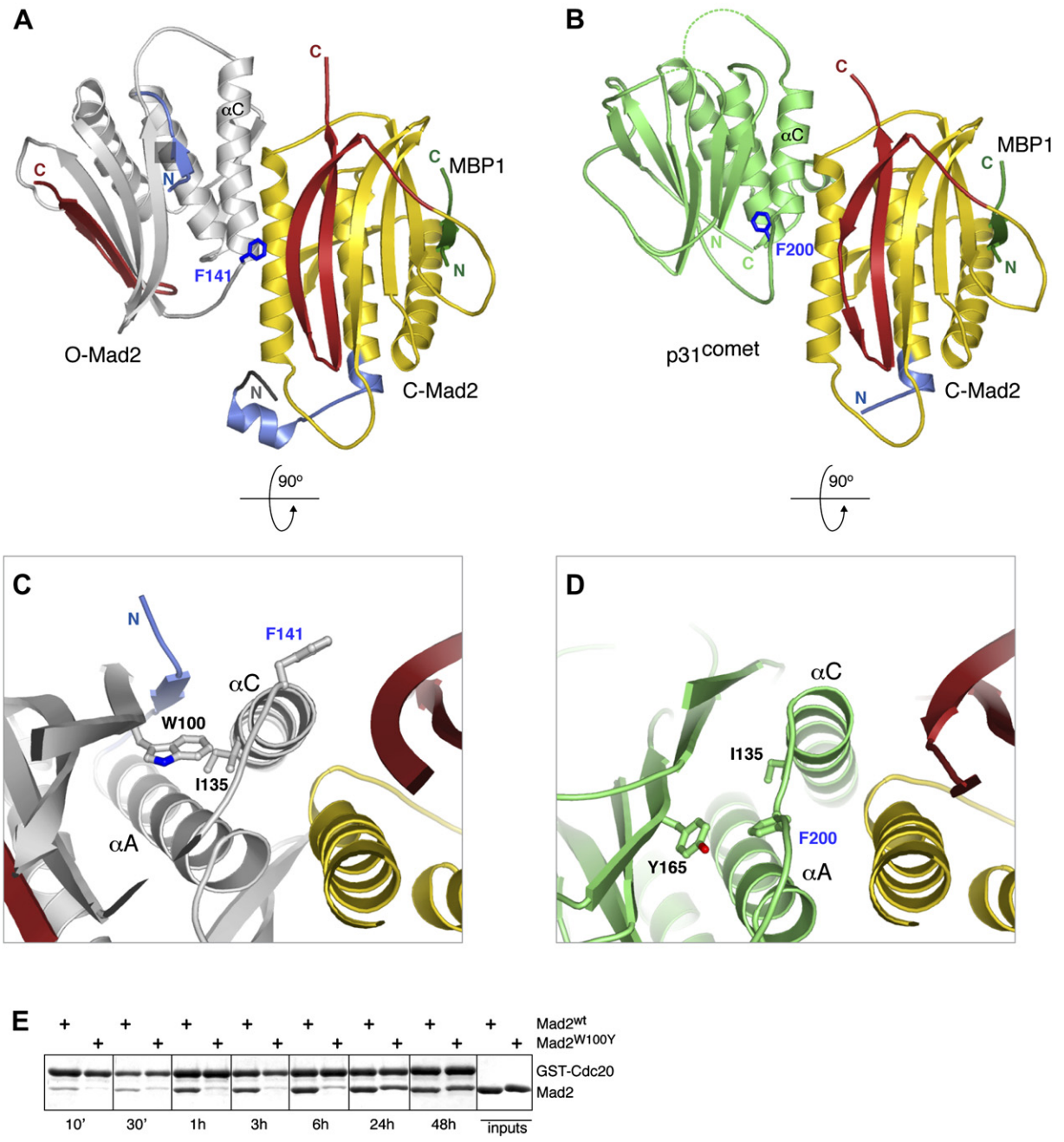

Figure 5. The p31^{comet}–C-Mad2 Complex and Its Relationship with O-Mad2–C-Mad2

(A) The O-Mad2–C-Mad2 complex is viewed as in Figure 1C.

(B) Ribbon diagram of the p31^{comet}–C-Mad2 complex (Yang et al., 2007). p31^{comet} is colored green. The orientation is the same as in (A).

(C) Close-up of the hydrophobic core of Mad2, showing the central position of Trp100 near the αC helix. The side chain of Phe141 points toward solvent.

(D) Tyr165 of p31^{comet} (equivalent to Trp100 of Mad2) is in very close contact with the side chain of Phe200, which is buried in p31^{comet} hydrophobic core. It is possible that the burial of Phe200 stabilizes a specific conformation of the hydrophobic core of p31^{comet} that contributes to its stronger binding to C-Mad2.

(E) Mutating Trp100 of Mad2 to Tyr (W100Y) generates a stable O-Mad2 mutant that binds to GST-Cdc20$^{111–138}$ with very slow kinetics.

O-Mad2 and that it fits more snugly to the C-Mad2 surface (see Figure 6B of Yang et al. [2007]). This correlates with a higher affinity of the interaction of p31^{comet} with C-Mad2 relative to O-Mad2 (Mapelli et al., 2006; Vink et al., 2006). In more detail, there is good structural overlap between p31^{comet} and O-Mad2 around the αC helices,

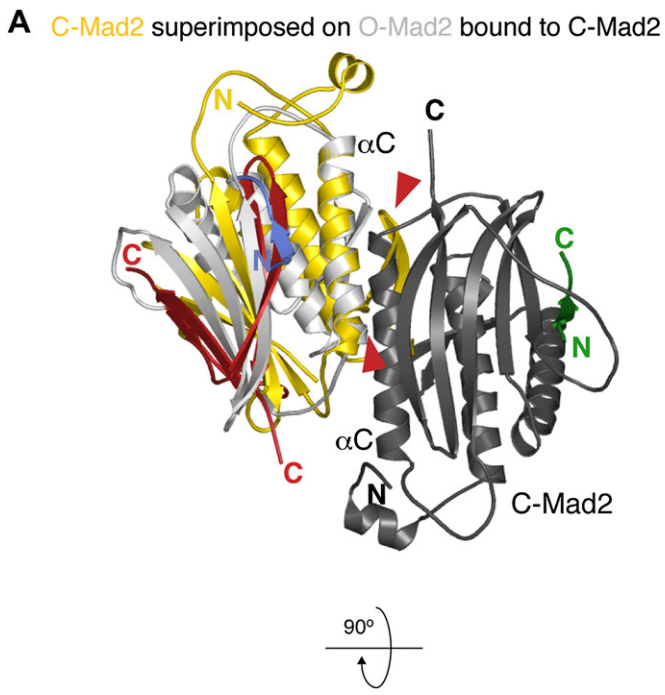

Figure 6. Superposition of O-Mad2 and C-Mad2

(A) On the left hand side, C-Mad2$^{O\text{-}Mad2}$ and O-Mad2 are superimposed and colored as in Figure 1. C-Mad2 is colored dark gray, and the MBP1 peptide (green). The segments used for the superposition are described in Experimental Procedures. The red arrowheads indicate points of steric clash between the O-Mad2-superimposed C-Mad2 in a hypothetical C-Mad2–C-Mad2 dimer.

(B) The view is 90° away from (A).

(C) Superposition of the independent views of C-Mad2 derived from the crystal structure of the conformational dimer described here and the structure of isolated C-Mad2 (i.e., not bound to O-Mad2) in the Mad1–C-Mad2 core complex (PDB ID Code 1GO4; [Sironi et al., 2002]) confirmed that C-Mad2 is a rigid scaffold, whose hydrophobic core remains essentially invariant even in the choice of side chain rotamers upon O-Mad2 binding (not shown).

suggesting that docking of the αC helices is essential for tight C-Mad2 binding (Yang et al., 2007). On the other hand, the αA helix of p31^{comet} and the following αAB helix (which is equivalent to the β2-β3 hairpin) make extensive contacts with C-Mad2 that are not observed for the equivalent elements of the O-Mad2–C-Mad2 interaction.

NMR chemical shift perturbation experiments revealed that O-Mad2 undergoes a global conformational change when incubated with C-Mad2 (Mapelli et al., 2006). Such change is consistent with the idea that C-Mad2 operates on O-Mad2 to create a conformational intermediate, I-Mad2, which might be expected to bind more readily to Cdc20. Indeed, the extensive conformational change that separates O-Mad2 from C-Mad2 is expected to imply significant activation energies, i.e., to be slow. This hypothesis found a first experimental confirmation (Luo et al., 2004). We have now confirmed that the forward rate constant (k_{on}) for the association of Mad2 with Cdc20 in the absence of Mad2 dimerization is 3–4 orders of magnitude slower that those that are normally observed for protein-protein interactions (M. Simonetta, R. Manzoni, M.M., L.M., S.S., A.M., and A. Ciliberto, unpublished data).

Within the framework defined in the previous paragraph, it is plausible that the deletion of the β5-αC loop in Mad2^{LL} locks O-Mad2 in a form that cannot undergo further change. Thus, we suspect that our structure provides a snapshot of the initial docking of O-Mad2 onto C-Mad2. We speculate that part of the binding energy from conformational dimerization of O-Mad2 with C-Mad2 might be used to trigger a conformational change in the Mad2 core required to convert the Mad2 topology. In this respect, the structure of the p31^{comet}–C-Mad2 complex might reveal certain aspects of the I-Mad2 intermediate. For instance, evident differences between p31^{comet} and O-Mad2 are that the αA and αC helices have a different reciprocal orientation, and that the αC helix of p31^{comet} is significantly shorter than the equivalent helix of O-Mad2 (Figures 5A and 5B). These changes correlate with the burial of Phe200 into the hydrophobic core of p31^{comet} (Figure 5D). The latter residue is equivalent to Phe141 of O-Mad2, which is fully exposed and is important for C-Mad2 binding to O-Mad2 (Figures 2 and 5D). It is possible that besides playing a role at the surface of C-Mad2, Phe141 of Mad2 represents a possible site of "communication" with the core of Mad2 that might be important for the stabilization of I-Mad2. In p31^{comet}, Phe200 is in van der Waals contact with Tyr165. The equivalent residue in Mad2 is Trp100, which is fully conserved in the Mad2 subfamily of HORMA domains. To test if this residue is important for the structural transition of Mad2, we mutated it into tyrosine (Mad2^{W100Y}). Mad2^{W100Y} is a very stable mutant that folds as O-Mad2 (Figure S3). We then tested the ability of Mad2^{W100Y} to bind Cdc20$^{111–138}$. In agreement with our hypothesis that Trp100 is important for the structural conversion of Mad2, Mad2^{W100Y} binds Cdc20 to levels that are comparable to those of wild-type Mad2, but the reaction has extremely slow kinetics, reaching equilibrium only after 48–72 hr (Figure 5E and data not shown). While an in-depth structural analysis will be required to understand the behavior of Mad2^{W100Y}, our results suggest that the hydrophobic core of Mad2 is an essential element of the Mad2 conformational change. Several other residues have different rotamers in the O-Mad2 and C-Mad2 hydrophobic core and define a possible chain starting at the αC helix and ending near the Mad2 C-terminal region (Figure 4C). In normal conditions (i.e., with wild-type O-Mad2), the docking of αC$^{O\text{-}Mad2}$-helix might have repercussions on the side chain of several hydrophobic residues in the vicinity of Leu13, such as Phe23, Ile128, and Ile135 favoring the extrusion of Leu13 from its position in the O-Mad2 core and accelerating the rate-limiting release of the β1-strand. In turn, this might correlate with rotations of other side chains, including those of Phe24, Ile28, and Phe151, to facilitate extrusion of the C-terminal tail (Figure 4C). A full analysis of this still speculative model of structural change in the Mad2 core will be the subject of our future studies.

Determinants of Asymmetric Binding

The binding pattern revealed by the O-Mad2–C-Mad2 and p31^{comet}–C-Mad2 complexes likely explains why O-Mad2 dimers are not observed (De Antoni et al., 2005a, 2005b; Nezi et al., 2006). Most likely, the inability to form O-Mad2 dimers is due to the fact that at least one C-terminal tail (from C-Mad2) is required at the dimer interface (Figure 1). Indeed, mutation of R184 prevents C-Mad2 from binding O-Mad2 (Figure 3F).

The observation that p31^{comet} has a topology that resembles C-Mad2 (Yang et al., 2007) might suggest that asymmetric C-Mad2 dimers similar to O-Mad2–C-Mad2 are possible. But rather than from the topology itself, the likelihood of an asymmetric dimerization of two C-Mad2 protomers should be evaluated on the quality of the fitting of the actual structures. We built a model of a C-Mad2–C-Mad2 dimer by superimposing the crystallographic model of C-Mad2 on O-Mad2 in the O-Mad2–C-Mad2 dimer. As O-Mad2 and p31^{comet} superimpose well on the αC helix (Figure S4 and data not shown), we modeled C-Mad2$^{O\text{-}Mad2}$ (the superscript indicates that this is the subunit superimposed on O-Mad2) based on the fitting of the αC helix. The model suggests that C-Mad2$^{O\text{-}Mad2}$ cannot be rigidly accommodated at the interface with C-Mad2–MBP1 due to steric clash between the β2-β3 hairpin and the αC helix of C-Mad2, and between the αA helix of C-Mad2$^{O\text{-}Mad2}$ and the αC helix of C-Mad2 at residue Gln134 (Figure 6B). These considerations suggest that asymmetric C-Mad2–C-Mad2 dimers similar to O-Mad2–C-Mad2 or to p31^{comet}–C-Mad2 are unlikely to form. It remains formally possible, however, that the binding interface can be molded to allow the formation of C-Mad2 dimers (Luo et al., 2004; Yu, 2006). Further biochemical and structural analyses will be required to shed light on this issue.

CONCLUSIONS

The Mad2 protein is endowed with an astonishing collection of unusual properties. Crystal structure determination of the Mad1–Mad2 complex revealed a safety belt binding mechanism and was instrumental for developing the "Mad2 template" model (Figure S1) (De Antoni et al., 2005a; Sironi et al., 2002). Strong evidence in favor of this model so far is that the stoichiometry and dynamics of the interaction of Mad2 with kinetochores can be faithfully reproduced with a purified system containing a stable Mad1–C-Mad2 complex (the kinetochore receptor) and O-Mad2 (the cytosolic component) (De Antoni et al., 2005a; Shah et al., 2004; Vink et al., 2006). This result indicates that conformational dimerization of Mad2 takes place at kinetochores. The structure of the Mad2 conformational dimer described here provides the first detailed view of the mechanism of binding of O-Mad2 to C-Mad2. The asymmetry of the Mad2 dimer is its most striking property, not only in the conformations of the two polypeptide chains but also in the chemical environment at the binding interface. Small deviations from 2-fold symmetry occur frequently at the interface of otherwise symmetric dimers (Brown, 2006). Fully asymmetric dimers, on the other hand, are rare. In the recently discovered example of the intracellular domain of the Epidermal Growth Factor Receptor (EGFR), an asymmetric dimer forms transiently upon EGF stimulation to activate the intracellular kinase domain (Zhang et al., 2006). The two EGFR subunits are probably chemically and conformationally identical and are therefore expected to have an equal chance to occupy either side of the asymmetric dimer. Certain aspects of Mad2 dimerization are reminiscent of the interaction of the major histocompatibility complex class II (MHC II) molecules with the peptide-editing factor DM. DM is structurally related to MHC II and acts on MHC II to catalyze the exchange of peptides in the peptide-binding groove of MHC II (Busch et al., 2005). But the asymmetric conformational dimer of Mad2 is probably unprecedented in the protein world, as in this case the interaction involves two structurally distinct Mad2 moieties endowed with the same sequence, and one of which folds stably as C-Mad2 after associating with Mad1 or Cdc20. Topological differences in the fold of the same protein are very rare. A notable example is that of the Serpins, whose latent and active states are characterized by the insertion or removal of a β strand in the middle of a β sheet (Whisstock and Bottomley, 2006). Future studies will have to address the idea that the C-Mad2 moiety acts as a catalyst to promote the modification of O-Mad2 into I-Mad2 required to bind Cdc20. The confirmation of this hypothesis poses very important technical challenges. The static structure of the Mad2 conformational dimer shown here cannot provide a definitive answer to this hypothesis, but is consistent with it. By identifying distinct changes in the Mad2 hydrophobic core that are required to support the Mad2 conformational change, and surface residues involved in dimerization, the structure illuminates the path for future experiments aimed to dissecting this problem.

EXPERIMENTAL PROCEDURES

Protein Biochemistry

Full-length HsMad2 and Mad2^{LL} were expressed with an N-terminal hexahistidine-tag from pET43 (Novagen) at 16°C in *E. coli* strain BL21-pLysS (DE3) for 12 hr after induction with 0.1 mM IPTG. Cells were lysed by sonication in 50 mM Tris-HCl (pH 8), 0.3 M NaCl, 5% glycerol, 5 mM imidazole and Roche Complete EDTA-free protease inhibitor cocktail. After clearing, the lysate was loaded on a HiTrap metal chelating column (GE Healthcare). Bound proteins were eluted with an imidazole gradient. Mad2 containing fractions were pooled, desalted, and loaded onto an anion-exchange (AE) Resource-Q column (GE Healthcare) equilibrated in 10 mM Tris-HCl (pH 8.0), 30 mM NaCl, 5% glycerol, 0.5 mM EDTA and 1 mM DTT. The protein was eluted using a NaCl gradient, concentrated by ultrafiltration, and further separated by size exclusion chromatography (SEC) on a Superdex-75 column (GE Healthcare) equilibrated in 10 mM Tris-HCl (pH 8), 0.1 M NaCl, 5% glycerol, 0.5 mM EDTA and 1 mM DTT. The entire purification scheme was carried out at 4°C.

Deletion of residues 109–117 was achieved by PCR amplification of the whole pET43 vector containing the Mad2 gene with the following phosphorylated primers: forward 5′-GGATCCGGAGAAAAGTCTCAG AAAGCTATCCAG, reverse 3′-CTTGTCACACTCAATATCAAACTG. After PCR, the methylated template was cleaved with the DpnI restriction enzyme. The PCR product was ligated and used to transform TOP10 competent cells (Invitrogen).

To assemble the O-Mad2–C-Mad2 dimer, synthetic MPB1 peptide was incubated with purified full-length Mad2^{wt} in a 5-fold molar excess for 1 hr at 20°C. A slight excess Mad2^{LL} was subsequently added and the incubation prolonged for an additional hour. The O-Mad2–C-Mad2 dimer was separated on a Superdex-75 (GE Healthcare) sizing column pre-equilibrated in 10 mM Tris-HCl (pH 8) and 0.1 M NaCl. Analytical SEC analyses were performed on a Superdex-75 column in a SEC buffer consisting of 20 mM Tris-HCl (pH 7.6), 0.1 M NaCl, 0.5 mM EDTA and 1 mM DTT. Analytical AE chromatography was carried out on a Resource-Q column on which pure proteins were loaded in 20 mM Tris-HCl (pH 7.6), 30 mM NaCl, 0.5 mM EDTA and 1 mM DTT, and eluted with a linear salt gradient up to 0.4 M in 15 column volumes at 4°C. Point mutations were introduced with QuikChange (Stratagene). C- and N- terminal deletion mutants were generated as previously described (Mapelli et al., 2006). All constructs were verified by sequencing.

Crystallization and Crystal Structure Determination

Crystallization experiments were performed with the sitting drop vapor diffusion technique at 20°C. 100 nl of protein solution at 43 mg/ml were mixed with 100 nl of reservoir solution with a Cartesian Honeybee liquid handler (Genomic Solutions). Crystals grew with a reservoir containing 0.1 M NaAcetate (pH 4.6) and 3.5 M NaFormate (SALTRX screen, Hampton Research). Crystals were flash-cooled in liquid N_2 without further optimization or cryo-protection. X-ray diffraction data were collected at beamline ID14-2 at ESRF (Grenoble, France). Data were indexed and scaled with HKL2000 (Otwinowski and Minor, 1997). Molecular Replacement (MR) was carried out with PHASER (McCoy et al., 2004) using the Mad2 chain of the Mad1–Mad2 crystallographic complex as a search model (PDB entry 1GO4). MR only located the three copies of C-Mad2, which were related by a proper 3-fold noncrystallographic symmetry axis. The 3-fold symmetry was subsequently exploited in DM (Collaborative Computational Project, 1994) for density modification. The 3-fold symmetry axis runs exactly through a Nickel atom coordinating the well-ordered His-tags of the C-Mad2 subunits. Model building of the open conformers was initiated with helical fragments placed into the modified electron density by the HelixBuild

module of ArpWarp (Morris et al., 2002). The model was then completed using iterative cycles of manual model building in Coot (Emsley and Cowtan, 2004) and restrained refinement in CNS (Brunger et al., 1998). Tight initial noncrystallographic symmetry restraints were relaxed at the end of the refinement. The three O-Mad2–C-Mad2 copies in the asymmetric unit are identical except for part of the C-terminal region of the open subunits, for which the density is rather poor.

Computational Analyses

For structural comparison of Mad2 conformers, sets of atoms belonging to the rigid core of the protein were first identified with ESCET (Schneider, 2002). All available closed Mad2 molecules (3 copies of the O-Mad2–C-Mad2 dimer and 4 copies of the Mad1–Mad2 complexes, PDB entry 1GO4) are classified as a single conformationally invariant fold, with no significant deviations in the main chain atom positions given the experimental uncertainties of the data. The same is true for the 3 copies of open Mad2 in the O-Mad2–C-Mad2 assembly. The largest structurally invariant region common to both open and closed conformers identified by ESCET is represented by residues 16–45, 54–84, 97–102, 142–147 and 155–161. This set of atoms representing the main rigid core of the Mad2 fold was used for least-square superposition of all conformers in O (Jones et al., 1991).

In Vitro Binding Assays

For GST-pulldown experiments in Figures 2–5, GST-Cdc20$^{111–138}$ was prepared as previously described (Sironi et al., 2002), and Mad2 mutants purified as detailed above. To test the effects of point mutation or deletion on the ability of Mad2 to bind Cdc20, 1 μM GST-Cdc20$^{111–138}$ pre-adsorbed on gluthatione (GSH) beads was incubated for 1 hr at 20°C with 2 μM of the chosen Mad2 construct in a buffer containing 10 mM HEPES (pH 7.5), 0.1 M NaCl, 0.5 mM EDTA and 1 mM DTT. Unbound Mad2 was washed away, and bound species resolved on SDS-PAGE. To monitor whether mutations impaired O-Mad2–C-Mad2 dimerization, C-Mad2 was formed by incubating the desired Mad2 species with GST-Cdc20$^{111–138}$ on GSH beads for 1 hr at 20°C (first addition). Then 2 μM of a second Mad2 moiety acting as an open conformer (Mad2$^{\Delta C}$) in the dimer assembly was added (second addition), and the incubation further protracted for 1 hr. After two washing steps, complexes immobilized on beads were analyzed by SDS-PAGE.

Supplemental Data

Supplemental Data include four figures, one table, and Supplemental References and can be found with this article online at http://www.cell.com/cgi/content/full/131/4/730/DC1/.

ACKNOWLEDGMENTS

We thank the Italian Association for Cancer Research (AIRC) and the Fondo di Investimento per la Ricerca di Base (FIRB) for support, the staff at the European Synchroton Radiation Facility (Grenoble, France) for assistance during data collection, Roberto Mosca for help with superpositions and Romilde Manzoni, Andrea Ciliberto, Kim Nasmyth, Jan-Michael Peters, and the members of the Musacchio laboratory for helpful discussions.

Received: May 3, 2007
Revised: June 28, 2007
Accepted: August 30, 2007
Published: November 15, 2007

REFERENCES

Aravind, L., and Koonin, E.V. (1998). The HORMA domain: a common structural denominator in mitotic checkpoints, chromosome synapsis and DNA repair. Trends Biochem. Sci. *23*, 284–286.

Brown, J.H. (2006). Breaking symmetry in protein dimers: designs and functions. Protein Sci. *15*, 1–13.

Brunger, A.T., Adams, P.D., Clore, G.M., DeLano, W.L., Gros, P., Grosse-Kunstleve, R.W., Jiang, J.-S., Kuszewski, J., Nilges, N., Pannu, N.S., et al. (1998). Crystallography and NMR system (CNS): A new software system for macromolecular structure determination. Acta Crystallogr. *D54*, 905–921.

Busch, R., Rinderknecht, C.H., Roh, S., Lee, A.W., Harding, J.J., Burster, T., Hornell, T.M., and Mellins, E.D. (2005). Achieving stability through editing and chaperoning: regulation of MHC class II peptide binding and expression. Immunol. Rev. *207*, 242–260.

Canman, J.C., Salmon, E.D., and Fang, G. (2002). Inducing precocious anaphase in cultured mammalian cells. Cell Motil. Cytoskeleton *52*, 61–65.

Chen, R.H., Brady, D.M., Smith, D., Murray, A.W., and Hardwick, K.G. (1999). The spindle checkpoint of budding yeast depends on a tight complex between the Mad1 and Mad2 proteins. Mol. Biol. Cell *10*, 2607–2618.

Chen, R.H., Shevchenko, A., Mann, M., and Murray, A.W. (1998). Spindle checkpoint protein Xmad1 recruits Xmad2 to unattached kinetochores. J. Cell Biol. *143*, 283–295.

Chung, E., and Chen, R.-H. (2002). Spindle Checkpoint Requires Mad1-bound and Mad1-free Mad2. Mol. Biol. Cell *13*, 1501–1511.

Cleveland, D.W., Mao, Y., and Sullivan, K.F. (2003). Centromeres and kinetochores: from epigenetics to mitotic checkpoint signaling. Cell *112*, 407–421.

Collaborative Computational Project, N. (1994). The CCP4 Suite: Programs for Protein Crystallography. Acta Crystallogr. *D50*, 760–763.

De Antoni, A., Pearson, C.G., Cimini, D., Canman, J.C., Sala, V., Nezi, L., Mapelli, M., Sironi, L., Faretta, M., Salmon, E.D., and Musacchio, A. (2005a). The mad1/mad2 complex as a template for mad2 activation in the spindle assembly checkpoint. Curr. Biol. *15*, 214–225.

De Antoni, A., Sala, V., and Musacchio, A. (2005b). Explaining the oligomerization properties of the spindle assembly checkpoint protein Mad2. Philos. Trans. R. Soc. Lond. B Biol. Sci. *360*, 637–647.

Emsley, P., and Cowtan, K. (2004). Coot: Model-Building Tools for Molecular Graphics. Acta Crystallogr. *D60*, 2126–2132.

Habu, T., Kim, S.H., Weinstein, J., and Matsumoto, T. (2002). Identification of a MAD2-binding protein, CMT2, and its role in mitosis. EMBO J. *21*, 6419–6428.

Hwang, L.H., Lau, L.F., Smith, D.L., Mistrot, C.A., Hardwick, K.G., Hwang, E.S., Amon, A., and Murray, A.W. (1998). Budding yeast Cdc20: a target of the spindle checkpoint. Science *279*, 1041–1044.

Jones, T.A., Zou, J.Y., Cowan, S.W., and Kjeldgaard, M. (1991). Improved methods for building protein models in electron density maps and the location of errors in these models. Acta Crystallogr. A *47*, 110–119.

Kallio, M., Weinstein, J., Daum, J.R., Burke, D.J., and Gorbsky, G.J. (1998). Mammalian p55CDC mediates association of the spindle checkpoint protein Mad2 with the cyclosome/anaphase-promoting complex, and is involved in regulating anaphase onset and late mitotic events. J. Cell Biol. *141*, 1393–1406.

Kim, S.H., Lin, D.P., Matsumoto, S., Kitazono, A., and Matsumoto, T. (1998). Fission yeast Slp1: an effector of the Mad2-dependent spindle checkpoint. Science *279*, 1045–1047.

Luo, X., Fang, G., Coldiron, M., Lin, Y., Yu, H., Kirschner, M.W., and Wagner, G. (2000). Structure of the mad2 spindle assembly checkpoint protein and its interaction with cdc20. Nat. Struct. Biol. *7*, 224–229.

Luo, X., Tang, Z., Rizo, J., and Yu, H. (2002). The Mad2 spindle checkpoint protein undergoes similar major conformational changes upon binding to either Mad1 or Cdc20. Mol. Cell *9*, 59–71.

Luo, X., Tang, Z., Xia, G., Wassmann, K., Matsumoto, T., Rizo, J., and Yu, H. (2004). The Mad2 spindle checkpoint protein has two distinct natively folded states. Nat. Struct. Mol. Biol. *11*, 338–345.

Maiato, H., Deluca, J., Salmon, E.D., and Earnshaw, W.C. (2004). The dynamic kinetochore-microtubule interface. J. Cell Sci. *117*, 5461–5477.

Mapelli, M., Filipp, F.V., Rancati, G., Massimiliano, L., Nezi, L., Stier, G., Hagan, R.S., Confalonieri, S., Piatti, S., Sattler, M., and Musacchio, A. (2006). Determinants of conformational dimerization of Mad2 and its inhibition by p31(comet). EMBO J. *25*, 1273–1284.

Martin-Lluesma, S., Stucke, V.M., and Nigg, E.A. (2002). Role of hec1 in spindle checkpoint signaling and kinetochore recruitment of mad1/mad2. Science *297*, 2267–2270.

McCoy, A.J., Storoni, L.C., and Read, R.J. (2004). Simple algorithm for a maximum-likelihood SAD function. Acta Crystallogr. *D60*, 1220–1228.

Otwinowski, Z., and Minor, W. (1997). Processing of X-ray Diffraction Data Collected in Oscillation Mode. In Methods in Enzymology, C.W. Carter, Jr. and M. Sweet, eds. (New York: Academic Press), pp. 307–326.

Morris, R.J., Perrakis, A., and Lamzin, V.S. (2002). ARP/wARP's model-building algorithms. I. The main chain. Acta Crystallogr. *D58*, 968–975.

Musacchio, A., and Salmon, E.D. (2007). The spindle-assembly checkpoint in space and time. Nat. Rev. Mol. Cell Biol. *8*, 379–393.

Nasmyth, K. (2005). How do so few control so many? Cell *120*, 739–746.

Nezi, L., Rancati, G., De Antoni, A., Pasqualato, S., Piatti, S., and Musacchio, A. (2006). Accumulation of Mad2–Cdc20 complex during spindle checkpoint activation requires binding of open and closed conformers of Mad2 in Saccharomyces cerevisiae. J. Cell Biol. *174*, 39–51.

Peters, J.M. (2006). The anaphase promoting complex/cyclosome: a machine designed to destroy. Nat. Rev. Mol. Cell Biol. *7*, 644–656.

Reddy, S.K., Rape, M., Margansky, W.A., and Kirschner, M.W. (2007). Ubiquitination by the anaphase-promoting complex drives spindle checkpoint inactivation. Nature *446*, 921–925.

Schneider, T.R. (2002). A genetic algorithm for the identification of conformationally invariant regions in protein molecules. Acta Crystallogr. D Biol. Crystallogr. *58*, 195–208.

Shah, J.V., Botvinick, E., Bonday, Z., Furnari, F., Berns, M., and Cleveland, D.W. (2004). Dynamics of centromere and kinetochore proteins; implications for checkpoint signaling and silencing. Curr. Biol. *14*, 942–952.

Sironi, L., Mapelli, M., Knapp, S., Antoni, A.D., Jeang, K.-T., and Musacchio, A. (2002). Crystal structure of the tetrameric Mad1-Mad2 core complex: implications of a 'safety belt' binding mechanism for the spindle checkpoint. EMBO J. *21*, 2496–2506.

Sironi, L., Melixetian, M., Faretta, M., Prosperini, E., Helin, K., and Musacchio, A. (2001). Mad2 binding to Mad1 and Cdc20, rather than oligomerization, is required for the spindle checkpoint. EMBO J. *20*, 6371–6382.

Stegmeier, F., Rape, M., Draviam, V.M., Nalepa, G., Sowa, M.E., Ang, X.L., McDonald, E.R., 3rd, Li, M.Z., Hannon, G.J., Sorger, P.K., et al. (2007). Anaphase initiation is regulated by antagonistic ubiquitination and deubiquitination activities. Nature *446*, 876–881.

Taylor, S.S., Scott, M.I., and Holland, A.J. (2004). The spindle checkpoint: a quality control mechanism which ensures accurate chromosome segregation. Chromosome Res. *12*, 599–616.

Vink, M., Simonetta, M., Transidico, P., Ferrari, K., Mapelli, M., De Antoni, A., Massimiliano, L., Ciliberto, A., Faretta, M., Salmon, E.D., and Musacchio, A. (2006). In Vitro FRAP Identifies the Minimal Requirements for Mad2 Kinetochore Dynamics. Curr. Biol. *16*, 755–766.

Whisstock, J.C., and Bottomley, S.P. (2006). Molecular gymnastics: serpin structure, folding and misfolding. Curr. Opin. Struct. Biol. *16*, 761–768.

Xia, G., Luo, X., Habu, T., Rizo, J., Matsumoto, T., and Yu, H. (2004). Conformation-specific binding of p31(comet) antagonizes the function of Mad2 in the spindle checkpoint. EMBO J. *23*, 3133–3143.

Yang, M., Li, B., Tomchick, D.R., Machius, M., Rizo, J., Yu, H., and Luo, X. (2007). Blockage of Mad2 Activation by p31come through Structural Mimicry. Cell *131*, this issue, 744–755.

Yu, H. (2006). Structural activation of Mad2 in the mitotic spindle checkpoint: the two-state Mad2 model versus the Mad2 template model. J. Cell Biol. *173*, 153–157.

Zhang, X., Gureasko, J., Shen, K., Cole, P.A., and Kuriyan, J. (2006). An allosteric mechanism for activation of the kinase domain of epidermal growth factor receptor. Cell *125*, 1137–1149.

Accession Numbers

Coordinates and structure factors of the Mad2 dimer have been deposited with the Protein Databank under ID code 2V64.